JACS
JOURNAL OF THE AMERICAN CHEMICAL SOCIETY
pubs.acs.org/JACS
Article

Selective Hydrofunctionalization of Alkenyl Fluorides Enabled by Nickel-Catalyzed Hydrogen Atoms and Group Transfer: Reaction Development and Mechanistic Study

Fan Chen,[§] Qianwei Zhang,[§] Yingying Li, Zhi-Xiang Yu,* and Lingling Chu*

Cite This: *J. Am. Chem. Soc.* 2024, 146, 11418−11431
Read Online

ABSTRACT: Due to the unique effect of fluorine atoms, the efficient construction of high-value alkyl fluorides has attracted significant interest in modern drug development. However, enantioselective catalytic strategies for the efficient assembly of highly functionalized chiral C(sp^3)-F scaffolds from simple starting materials have been underutilized. Herein, we demonstrate a nickel-catalyzed radical transfer strategy for the efficient, modular, asymmetric hydrogenation and hydroalkylation of alkenyl fluorides with primary, secondary, and tertiary alkyl halides under mild conditions. The transformation provides facile access to various structurally complex secondary and tertiary α-fluoro amide products from readily available starting materials with excellent substrate compatibility and distinct selectivity. Furthermore, the utility of this method is demonstrated by late-stage modifications and product derivatizations. Detailed mechanistic studies and DFT calculations have been conducted, showing that the rate-determining step for asymmetric hydrogenation reaction is NiH-HAT toward alkenyl fluorides and the stereo-determining step is alcohol coordination to Ni-enolates followed by a barrierless protonation. The mechanism for the asymmetric hydroalkylation reaction is also delivered in this investigation.

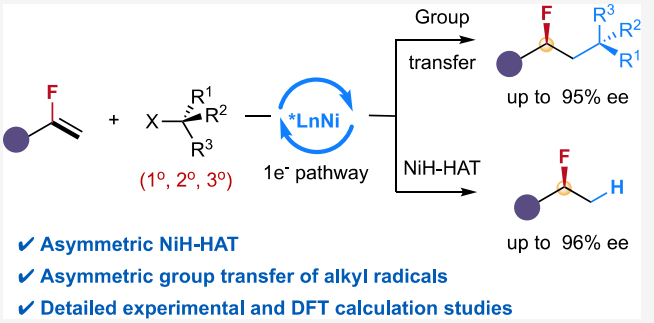

INTRODUCTION

The incorporation of fluorine atoms is well-known to modulate the physicochemical and biological properties of small molecules relevant to medicine and life sciences, including lipophilicity, biostability, and bioavailability.[1] Of these, three-dimensional alkyl fluoride motifs are particularly interesting but are less abundant. Compared to aromatic fluorides, alkyl fluorides are more structurally diverse, the exploration of which is becoming an increasingly crucial aspect of modern drug development.[2] Consequently, C(sp^3)-F units have been increasingly used in several marketed pharmaceutics, including Azvudine (treatment of HIV), Clevudine (treatment of hepatitis B), [^{18}F]FDG (radiochemistry tracer), Fluticasone propionate (treatment of asthma), and Flurithromycin (treatment of infections).[3] Nevertheless, the use of alkyl fluorides in drug development is exacerbated by methodological limitations. As a result, the development of catalytic, selective methods to access structurally complex, high-value alkyl fluorides, particularly those with stereodefined fluorinated centers, is still an active area of research.[4] In the past few decades, enantioselective direct fluorination reactions have been extensively studied as a powerful platform for the construction of C(sp^3)−F bonds from carbonyls, alkenes, and their analogs.[5] An alternative strategy involves transition-metal-catalyzed asymmetric cross-couplings of F-incorporated motifs, such as fluorinated enolates (or their equivalents) and α-fluoro alkyl halides, to form the desired C−F stereocenters.[6] Moreover, alkenyl fluorides, one of the most readily available F-containing building blocks, have also been explored as simple precursors for stereodefined C(sp^3)−F motifs, typically via catalytic asymmetric hydrogenation.[7] Recently, Sigman et al., via Pd-catalyzed asymmetric remote hydroarylation,[8] and Fu et al., via Co-catalyzed asymmetric hydroalkylation with alkyl halides,[9] have disclosed two examples of catalytic asymmetric hydrofunctionalization of alkenyl fluorides (Figure 1a). However, the α-F-alkylmetal intermediates involved in such an organometallic strategy are prone to undergoing a competitive defluorination process to give undesired non-fluorinated compound.[10] As a result, the development of a catalytic, mechanistically distinct strategy that bypasses the defluorination process to facilitate the enantioselective hydrofunctionalization of alkenyl fluorides of readily diversifiable

Received: January 30, 2024
Revised: March 23, 2024
Accepted: March 25, 2024
Published: April 15, 2024

https://doi.org/10.1021/jacs.4c01506
J. Am. Chem. Soc. 2024, 146, 11418−11431

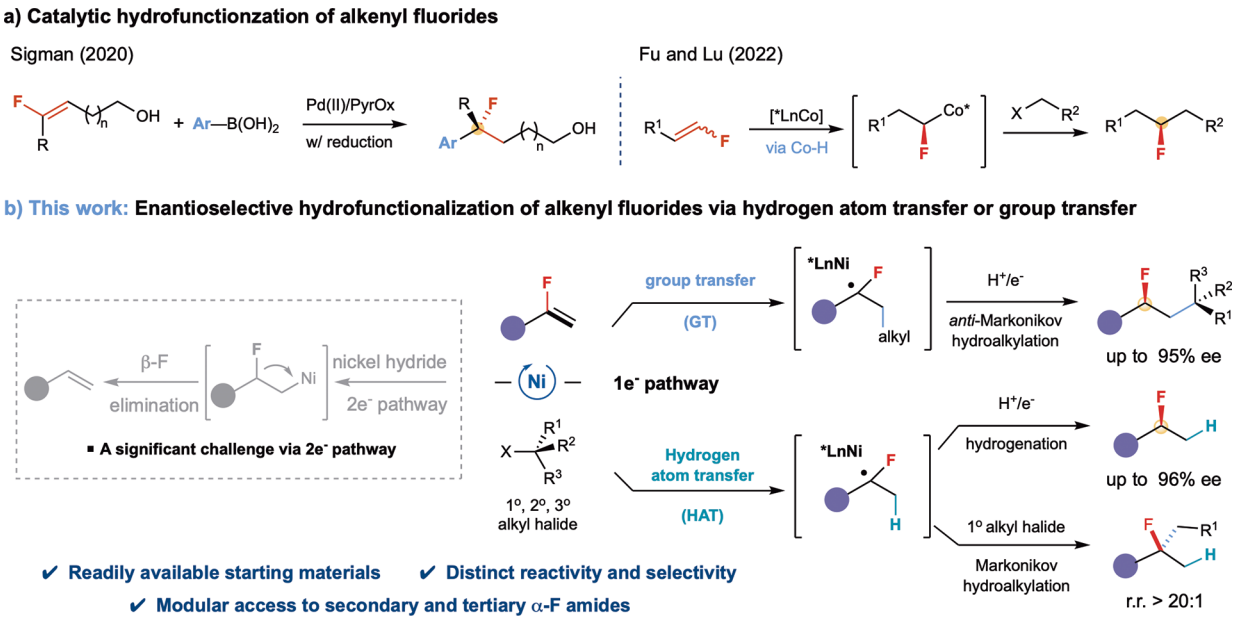

Figure 1. Asymmetric construction of fluorinated stereocenters. (a) Catalytic hydrofunctionalization of alkenyl fluorides. (b) Construction of secondary and tertiary fluorinated stereocenters via the nickel-catalyzed hydrogen atom and group transfer process.

scaffolds while ensuring stereoselectivity remains an elusive yet essential objective.

Recently, metal hydride hydrogen atom transfer (MH–HAT) catalysis has emerged as a potent yet distinct platform for the selective hydrogenation and hydrofunctionalization reactions of alkenes via radical processes with complementary reactivity and selectivity.[11,12] Typically, this strategy proceeds via HAT to alkenes followed by radical trappings or metal-catalyzed cross-couplings of the alkyl radicals produced.[13] Motivated by this chemistry, we hypothesized that such a radical transfer process would provide a viable approach for the selective functionalization of alkenyl fluorides under mild conditions without the need for defluorination.[11b] As a continuation of our research interest in nickel-catalyzed radical asymmetric functionalization of alkenes,[14] precisely, we speculated that nickel-catalyzed HAT[10c,15] or group transfer of alkyl radicals[16] to alkenyl fluorides would generate α-fluoro radical/Ni cage pair, which could engage in stereoselective protometalation or cross-couplings with organohalides in the presence of chiral nickel complexes.[17] If successful, this innovative strategy would not only enable efficient and facile access to fluorinated sp^3 stereocenters from planar alkenyl fluorides, but it would also complement the previously well explored nickel-hydride-catalyzed asymmetric hydroalkylation of alkenes (which is predominantly limited to primary and secondary alkyl electrophiles),[18,19] with distinct selectivity and an expanded reservoir of alkyl halides. Accordingly, we report the successful execution of radical-transfer-enabled asymmetric hydrogenation and hydroalkylation of alkenyl fluorides with tertiary, secondary, and primary alkyl halides to access structurally diverse, enantioenriched secondary and tertiary α-fluoro amides via nickel catalysis (Figure 1b).

RESULTS AND DISCUSSION

We began our investigations by exploring the asymmetric alkyl transfer reaction of α-fluoro alkenyl amide **1a** with *tert*-butyl bromide in the presence of various nickel catalysts, chiral ligands, and reductants. The experiments revealed that the formation of the enantioenriched secondary α-fluoro amide **2a** was feasible with the combination of catalytic $NiBr_2 \cdot (PPh_3)_2$, chiral tridentate Pybox ligands, and $(MeO)_3SiH$ in the presence of K_3PO_4 as a base, with isopropyl alcohol and ZnI_2 as the additives (Table 1). Furthermore, with (*S*,*S*)-**L1**, the coupling product **2a** was obtained in 78% yield and 91% ee, along with the hydrogenation product **3a** in 26% yield and 51% ee (entry 1). In this instance, no Markov–Nakov hydroalkylation product was observed. Accordingly, we found that the side chains of Pybox were crucial to the performance of product **2a** (entries 2–9). Moreover, increasing or decreasing the steric hindrance of the alkyl chains (such as *tert*-butyl, isopropyl, cyclohexyl, and diphenylmethyl) resulted in varying degrees of reduced yields and enantiomeric excess (entries 2–5). In addition, replacing the two alkyl chains with two phenyl groups resulted in neither alkylation product **2a** nor hydrogenation product **3a** being observed (entry 6). In this reaction, Pybox ligands with different substituents on the pyridine ring or oxazoline groups were less effective (entries 7–9). Moreover, switching the chiral bisoxazoline (BiOx) groups to the more electron-rich chiral biimidazoline (BiIm) groups had no positive effect (entry 10). On the other hand, the use of other bidentate chiral ligands, such as BiOx [(*S*,*S*)-**L11**], BiIm [(*S*,*S*)-**L12**], and Box [(*S*,*S*)-**L13**]] ligands, failed with low or no enantioselectivity (entries 11–13). Control experiments indicated the necessity of nickel catalyst, ligand, silane, and base; simultaneously, a substantial amount of racemic **3a** was observed in the absence of a ligand, highlighting the difficulty of achieving asymmetric hydrogenation of alkenyl fluorides (entries 14 and 15). Utilizing alcohol and ZnI_2 as additives improved the yield and enantioselectivity of product **2a** (entries 16 and 17). Without ZnI_2, we observed a significant increase in the enantioselectivity of compound **3a** (entry 17). Encouraged by this result, we further evaluated the reaction conditions (e.g., nickel salts and solvents) and found that the combination of $NiCl_2 \cdot DME$/(*S*,*S*)-**L1** in tetrahydrofuran/*N*-methyl-2-pyrrolidone (NMP) furnished enantioenriched **3a** in 95% yield and 91% ee (entry

https://doi.org/10.1021/jacs.4c01506
J. Am. Chem. Soc. 2024, 146, 11418–11431

Table 1. Optimization of the Reaction Conditions[b]

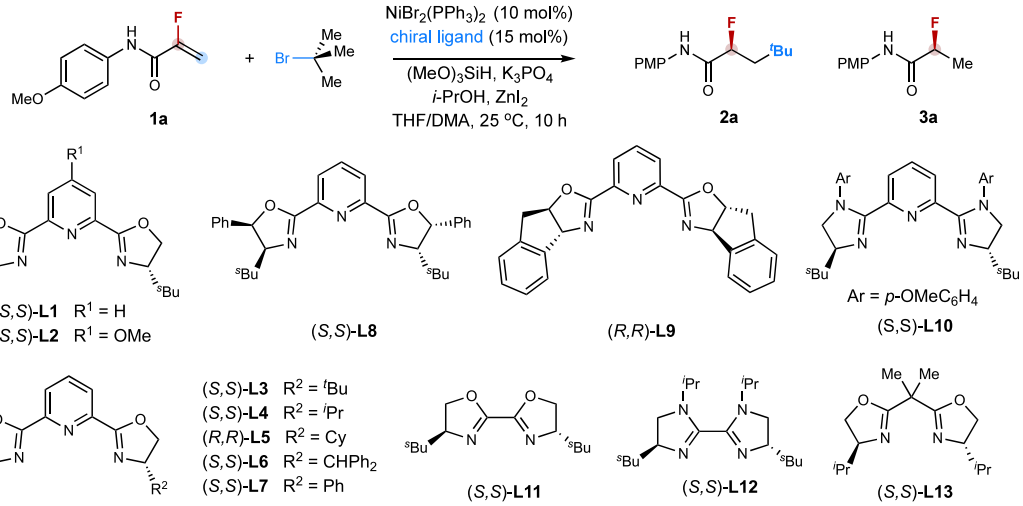

Entry	Conditions	Yield of 2a	ee of 2a	Yield of 3a	ee of 3a
1	(*S, S*)-**L1**	78%	91%	26%	51%
2	(*S, S*)-**L3**	60%	18%	10%	36%
3	(*S, S*)-**L4**	82%	86%	25%	45%
4	(*R, R*)-**L5**	51%	−53%	26%	−33%
5	(*S, S*)-**L6**	48%	82%	12%	29%
6	(*S, S*)-**L7**	8%	0%	trace	--
7	(*S, S*)-**L2**	20%	37%	29%	11%
8	(*S, S*)-**L8**	51%	68%	7%	40%
9	(*R, R*)-**L9**	44%	−12%	11%	−2%
10	(*S, S*)-**L10**	66%	12%	8%	6%
11	(*S, S*)-**L11**	13%	2%	16%	6%
12	(*S, S*)-**L12**	57%	33%	13%	2%
13	(*S, S*)-**L13**	16%	0%	36%	0%
14	no Ni, silane, or K_3PO_4	0%	--	0%	--
15	no ligand	0%	--	47%	0%
16	no *i*-PrOH	30%	82%	38%	62%
17	no ZnI_2	62%	91%	26%	89%
18[a]	$NiCl_2$·DME/ (*S, S*)-**L1**	trace	--	95%	91%

[a]With *α*-fluoro alkene **1a** (0.1 mmol), *tert*-butyl bromide (0.2 mmol), *i*-PrOH (3.0 equiv), THF/NMP (v/v = 4:1, 0.04 M). [b]Reaction conditions: *α*-fluoro alkene **1a** (0.15 mmol), *tert*-butyl bromide (0.1 mmol), $NiBr_2$·$(PPh_3)_2$ (10 mol %), (*S,S*)-**L1** (15 mol %), K_3PO_4 (1.0 equiv), $(MeO)_3SiH$ (2.0 equiv), *i*-PrOH (8.0 equiv), ZnI_2 (0.3 equiv), THF/DMA (v/v = 7:3, 0.05 M), 25 °C, 10 h. GC yields were determined using *n*-dodecane as an internal standard, and the ee values were determined using high-performance liquid chromatography on a chiral stationary phase.

18). The use of $NiCl_2$·DME without associated or added triphenylphosphine was deemed essential for achieving high efficiency of hydrogenation product **3a** (see the Supporting Information for details).

Having determined the optimal conditions, we investigated the generality of this asymmetric alkyl transfer reaction regarding alkenyl fluorides. As shown in Figure 2, a series of *α*-fluoro acrylamides with electron-rich or electron-poor aromatic substituents on the nitrogen atom underwent efficient and selective couplings with *tert*-butyl bromide under mild conditions, furnishing the desired chiral secondary *β*-alkyl-*α*-fluoro amides with high yields, exclusive regioselectivity, and good to excellent enantioselectivity (**2a**−**2r**, up to 94% ee). In addition, the electronic properties of the *N*-aryl substituents played a crucial role in reaction efficiency, and acrylamides with more electron-rich arenes resulted in greater ee values

https://doi.org/10.1021/jacs.4c01506
J. Am. Chem. Soc. 2024, 146, 11418−11431

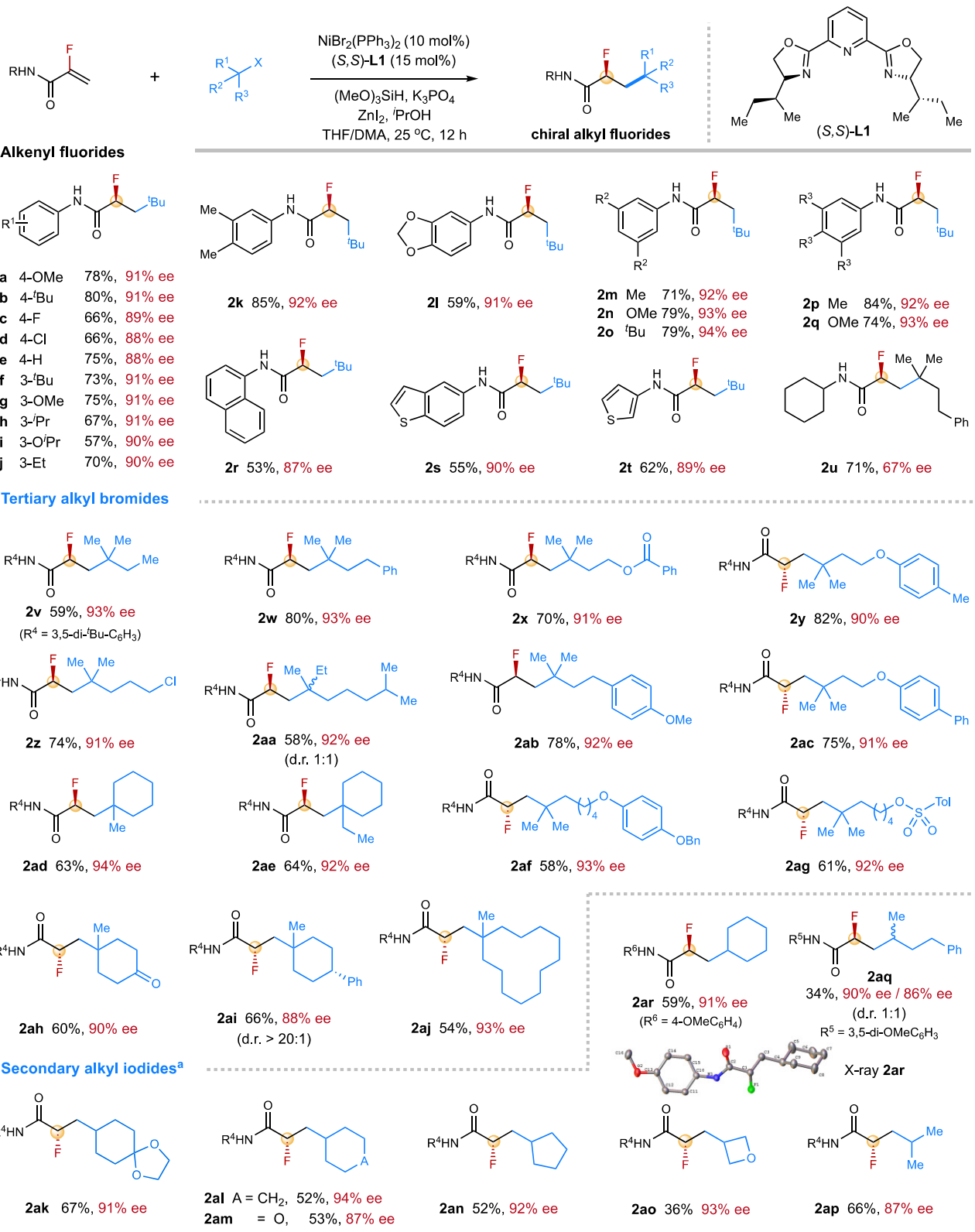

Figure 2. Substrate scope for the asymmetric group transfer of alkyl radicals. Reaction conditions for tertiary alkyl bromides: α-fluoro alkene (0.15 mmol), alkyl halide (0.1 mmol), $NiBr_2{\cdot}(PPh_3)_2$ (10 mol %), (*S*,*S*)-**L1** (15 mol %), K_3PO_4 (1.0 equiv), $(MeO)_3SiH$ (2.0 equiv), *i*-PrOH (8.0 equiv), ZnI_2 (0.3 equiv), THF/DMA (7:3, 0.05 M), 25 °C, 10 h. [a]w/$NiBr_2{\cdot}$DME (10 mol %), alkyl iodide, *i*-PrOH (2.0 equiv), TMEDA (0.3 equiv), EtOAc/DMA (4:1, 0.05 M).

(**2n**−**2q**, up to 94% ee). In the case of naphthalenyl acrylamides (**2r**, 87% ee), steric hindrance of N-aryl substituents had a minor effect on the enantioselectivity. *N*-heteroaryl substitutions were compatible (**2s**−**2t**, 89−90% ee), whereas *N*-alkyl substituted acrylamides had decreased ee values (**2u**, 67% ee).

A wide range of alkyl halides can be applied with this catalytic asymmetric alkyl transfer reaction (Figure 2).

https://doi.org/10.1021/jacs.4c01506
J. Am. Chem. Soc. 2024, 146, 11418−11431

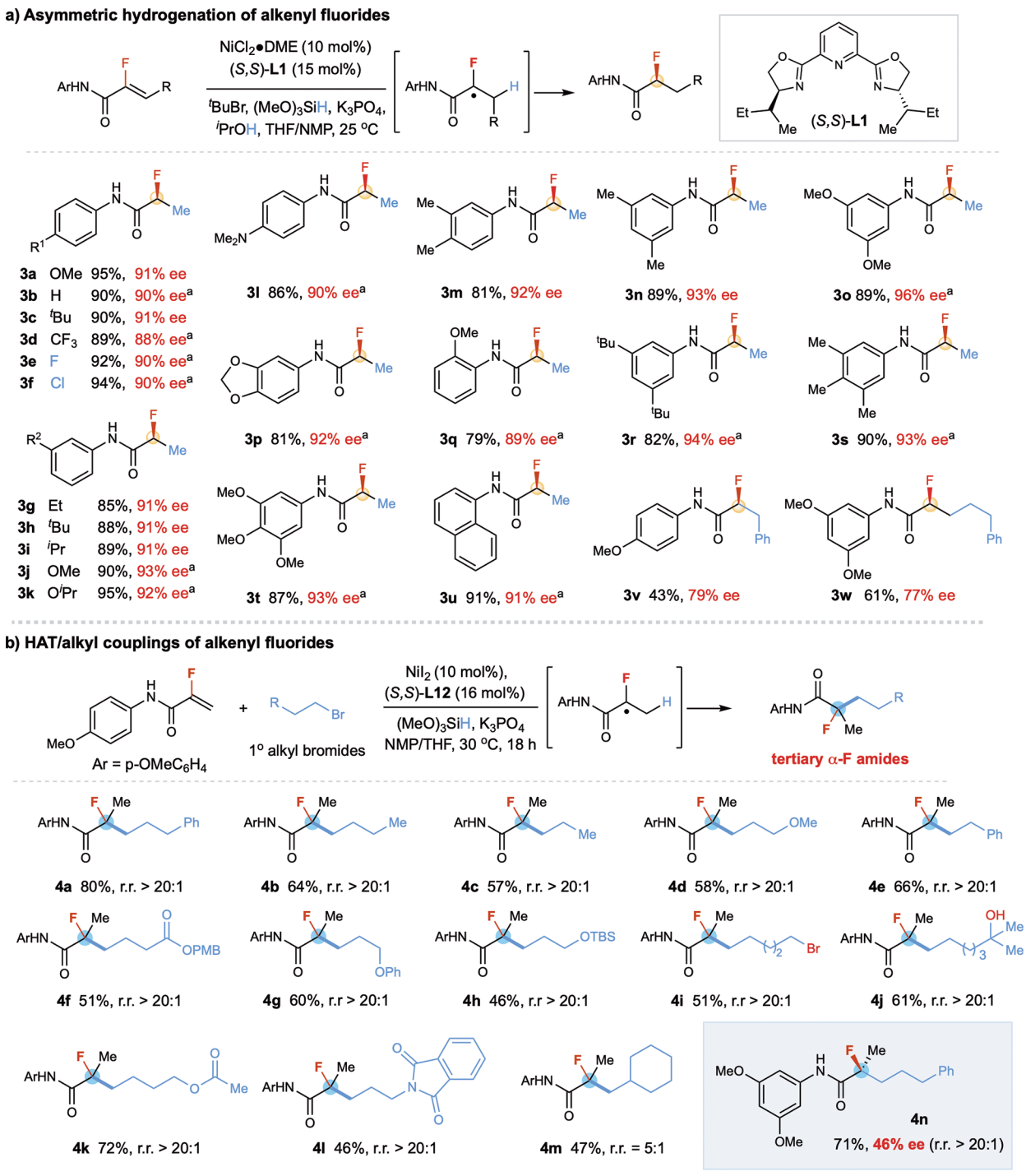

Figure 3. Substrate scope for hydrogen atom transfer. (a) Asymmetric hydrogenation. (b) HAT/alkyl coupling. Reaction conditions for hydrogenation: α-fluoro alkene (0.1 mmol), *tert*-butyl bromide (0.2 mmol), $NiCl_2$·DME (10 mol %), (*S*,*S*)-**L1** (15 mol %), K_3PO_4 (1.0 equiv), $(MeO)_3SiH$ (2.0 equiv), *i*-PrOH (3.0 equiv), THF/NMP (v/v = 4:1, 0.04 M), 25 °C, 10 h. [a]The reactions were carried out at 0 °C. Reaction conditions for hydroalkylation: α-fluoro alkene (0.1 mmol), primary alkyl bromide (0.12 mmol), NiI_2 (10 mol %), (*S*,*S*)-**L12** (16 mol %), K_3PO_4 (2.0 equiv), $(MeO)_3SiH$ (2.0 equiv), NMP/THF (v/v = 3:1, 0.04M), 30 °C, 18 h.

Correspondingly, a wide variety of linear tertiary alkyl bromides could produce the desired enantioenriched α-fluoro amides in good yields and high enantiomeric excess (**2v**−**2aj**, up to 94% ee). The couplings with cyclic tertiary alkyl bromides, including substituted cyclohexyl and cylcododecanyl bromides, also proceeded with a high enantiomeric excess (**2ad and 2ae**, **2ah**−**2aj**, as high as 94% ee). In addition, several common functional groups, including alkyl chlorides, esters, ethers, sulfonates, and ketones, could tolerate the mild conditions (**2x**−**2z, 2ac, 2af**−**2ah**, up to 93% ee). Moreover, both alkyl bromides and iodides were competent coupling partners, with tertiary alkyl bromides yielding a slightly greater enantiomeric excess than did iodides (Table S9). Incorporating cyclic and acyclic secondary alkyl iodides into a catalytic system containing ethyl acetate/dimethylacetamide as the solvent also furnished the alkyl transfer products with

https://doi.org/10.1021/jacs.4c01506
J. Am. Chem. Soc. 2024, 146, 11418−11431

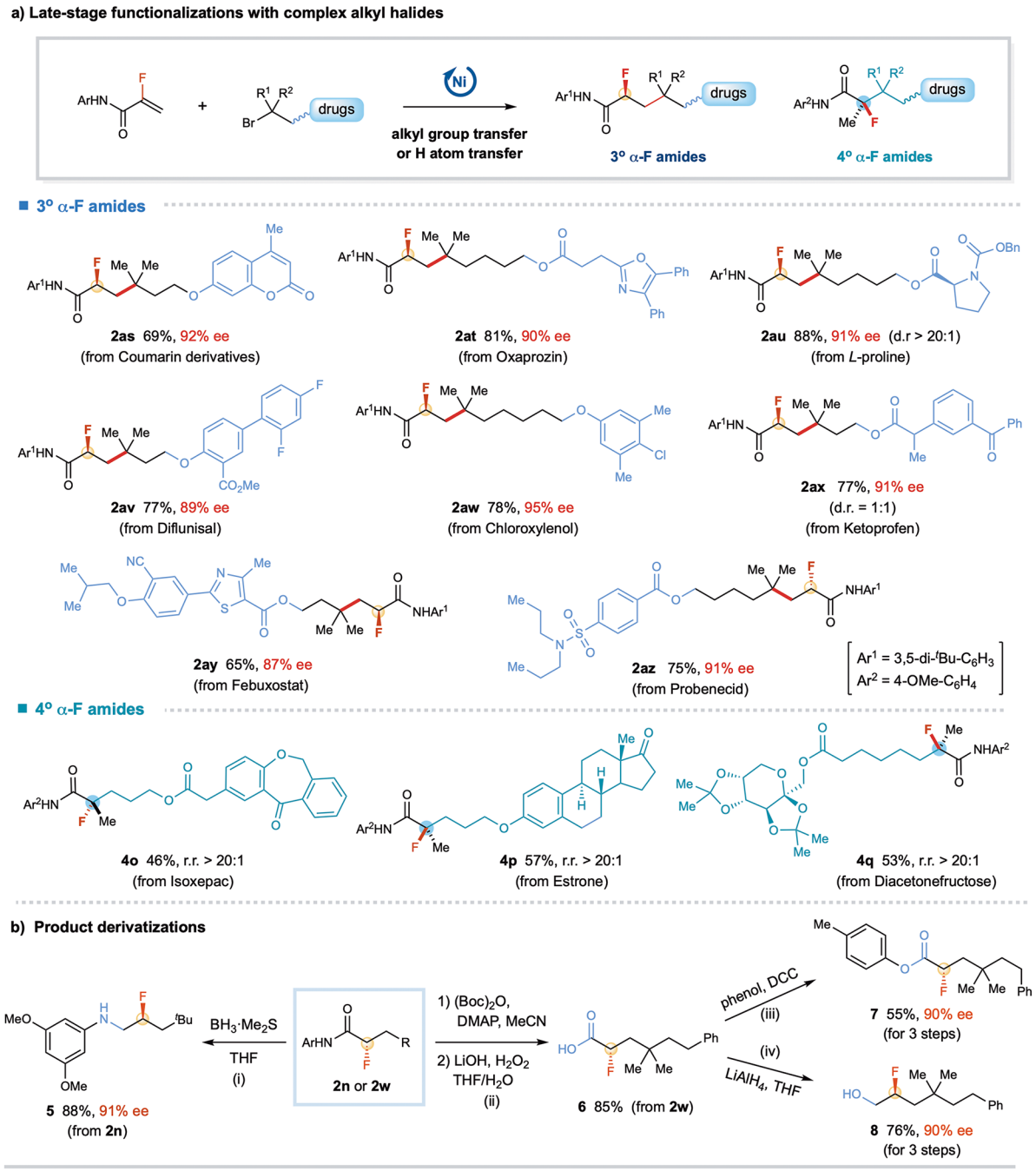

Figure 4. Synthetic applications. (a) Late-stage functionalizations with complex alkyl halides; (b) product derivatizations. Reaction conditions: (i) $BH_3{\cdot}Me_2S$, THF, 0 °C to reflux. (ii) (1) $(Boc)_2O$, 4-dimethylaminopyridine (DMAP), MeCN, 70 °C; (2) LiOH, H_2O_2, THF/H_2O = 3:1, 0 °C to rt. (iii) *p*-MePhOH, dicyclohexylcarbodiimide, DMAP, dichloromethane, rt. (iv) $LiAlH_4$, THF, 0 °C to rt. For detailed reaction conditions, see the Supporting Information.

satisfactory yields and generally good enantiomeric excess (**2ak**−**2ar**, up to 94% ee). The reaction with racemic secondary alkyl iodide, as illustrated by **2aq**, also generated a chiral α-fluoro amide in good enantiomeric excess, albeit with a low diastereomeric ratio. This asymmetric alkyl transfer reaction proceeded exclusively with *anti*-Markovnikov selectivity in every instance. Subsequently, the absolute configuration of product **2ar** was determined using X-ray single-crystal diffraction.

Next, we investigated the generality of the asymmetric hydrogenation protocol in entry 18 of Table 1. As shown in Figure 3a, a wide variety of α-fluoro acrylamides were converted with high yields and excellent enantiomeric excess to the corresponding secondary α-fluoro amides. Conventionally, acrylamides with more electron-rich aromatics (**3a**−**3u**, up to 96% ee) were more efficient. Furthermore, internal fluorinated acrylamides were suitable substrates, albeit with reduced enantioselectivity (**3v**−**3w**, up to 79% ee). This catalytic system provides a pathway for the asymmetric hydrogenation of alkenyl fluorides with two synthetically advantageous features: (i) not requiring hydrogen gas or

https://doi.org/10.1021/jacs.4c01506
J. Am. Chem. Soc. 2024, 146, 11418−11431

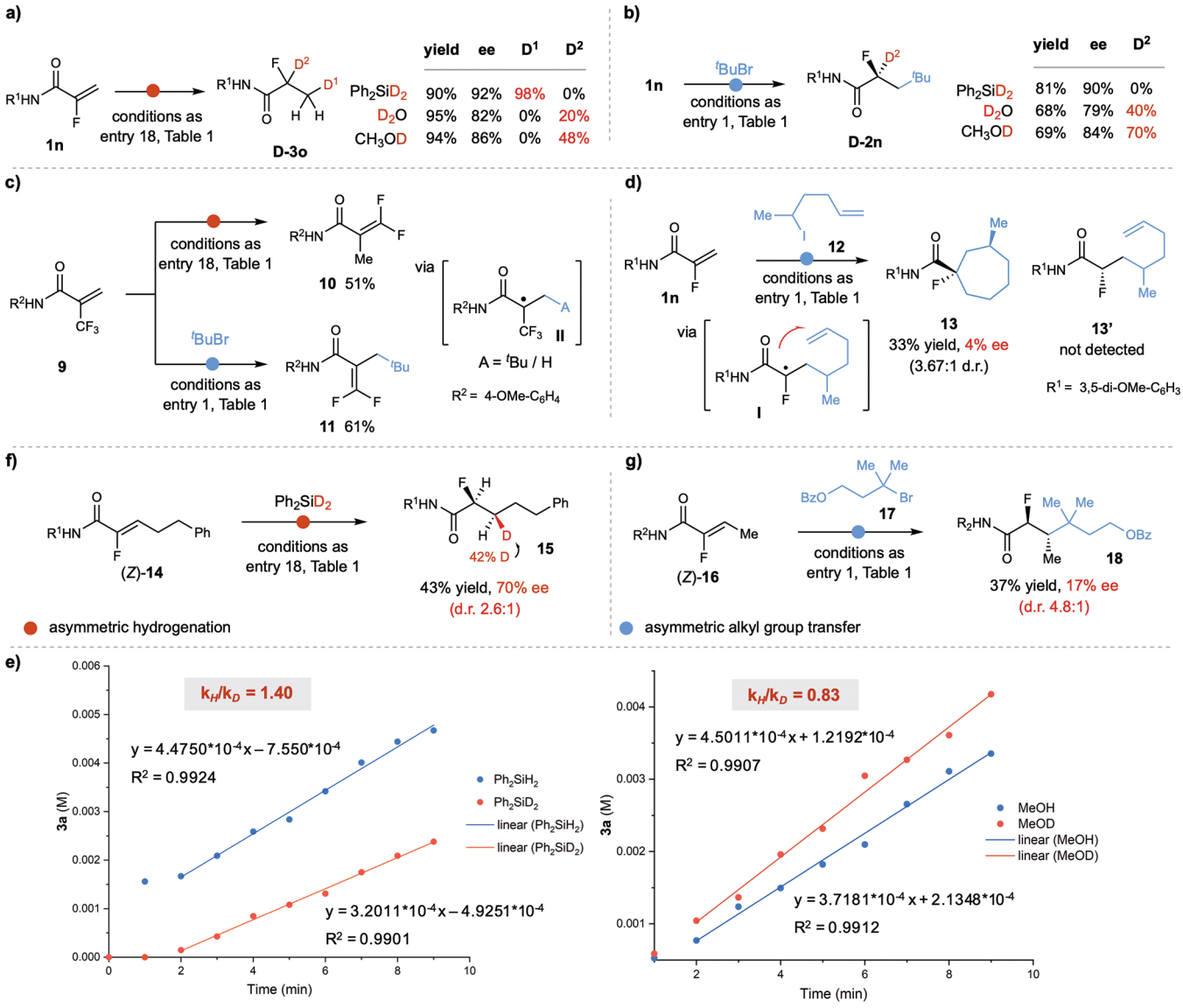

* For the hydrogenation reaction of **1a** under the condition as entry 18, Table 1

Figure 5. Mechanistic studies. (a) Deuterium-labeling experiments for hydrogenation reaction; (b) deuterium-labeling experiments for alkyl transfer reaction; (c) reactions with CF_3-alkenes; (d) radical probe reactions for alkyl transfer reaction; (e) kinetic isotope effect experiments for hydrogenation reactions; (f) hydrogenation reaction of internal alkenes; and (g) alkyl transfer reaction with internal alkenes.

precious metal catalysts;[7b,c] (ii) not producing defluorination byproducts.[11b]

Inspired by Shenvi's recent work in which a combination of MH−HAT and Ni-catalyzed aryl couplings was utilized to achieve Markovnikov-selective hydroarylation,[11c,13a] we reason that the α-fluoro radical, generated via nickel hydride HAT in our system, could further undergo Ni-mediated cross-couplings with organic halides, thereby delivering hydrofunctionalization products with tertiary fluorinated stereogenic centers. We found that Ni-catalyzed branch-selective hydroalkylation of alkenyl fluorides was feasible by employing less sterically hindered primary alkyl halides as coupling partners in the presence of catalytic NiI_2 and a bidentate and more electron-rich ligand bisimidazole (*S*,*S*)-**L12** (see Tables S17−S19 for optimization details). Notably, this radical transfer protocol offered distinct regioselectivity to the nickel hydride-enabled hydroalkylation of acrylamides.[19e] As depicted in Figure 3b, numerous primary alkyl bromides underwent efficient couplings with alkenyl fluoride **1a**, resulting in the formation of tertiary α-fluoro amides with high yields and excellent Markovnikov selectivity (**4a**−**4n**, r.r. > 20:1). Tethered aromatics, ethers, esters, silicons, bromides, and even free alcohols were all compatible, providing potential synthetic manipulation handles (**4d**, **4f**−**4k**). The selective and efficient coupling of one bromo atom to 1,5-dibromopentane left the other bromide uncoupled (**4i**). In addition, this protocol yielded enantioenriched tertiary α-fluoro amide products with high yield and excellent enantiomeric excess (**4n**, 46% ee). In contrast to previous work, which typically needs one metal catalyst for MH−HAT and another metal catalyst for radical couplings, this reaction uses a single nickel catalyst for both HAT and cross-coupling processes.[13a,b,d,e]

To demonstrate the synthetic utility of this asymmetric radical transfer protocol, particularly in the late-stage synthesis of complex bioactive chiral fluorinated motifs, several alkyl halides derived from natural products and biologically active

https://doi.org/10.1021/jacs.4c01506
J. Am. Chem. Soc. 2024, 146, 11418−11431

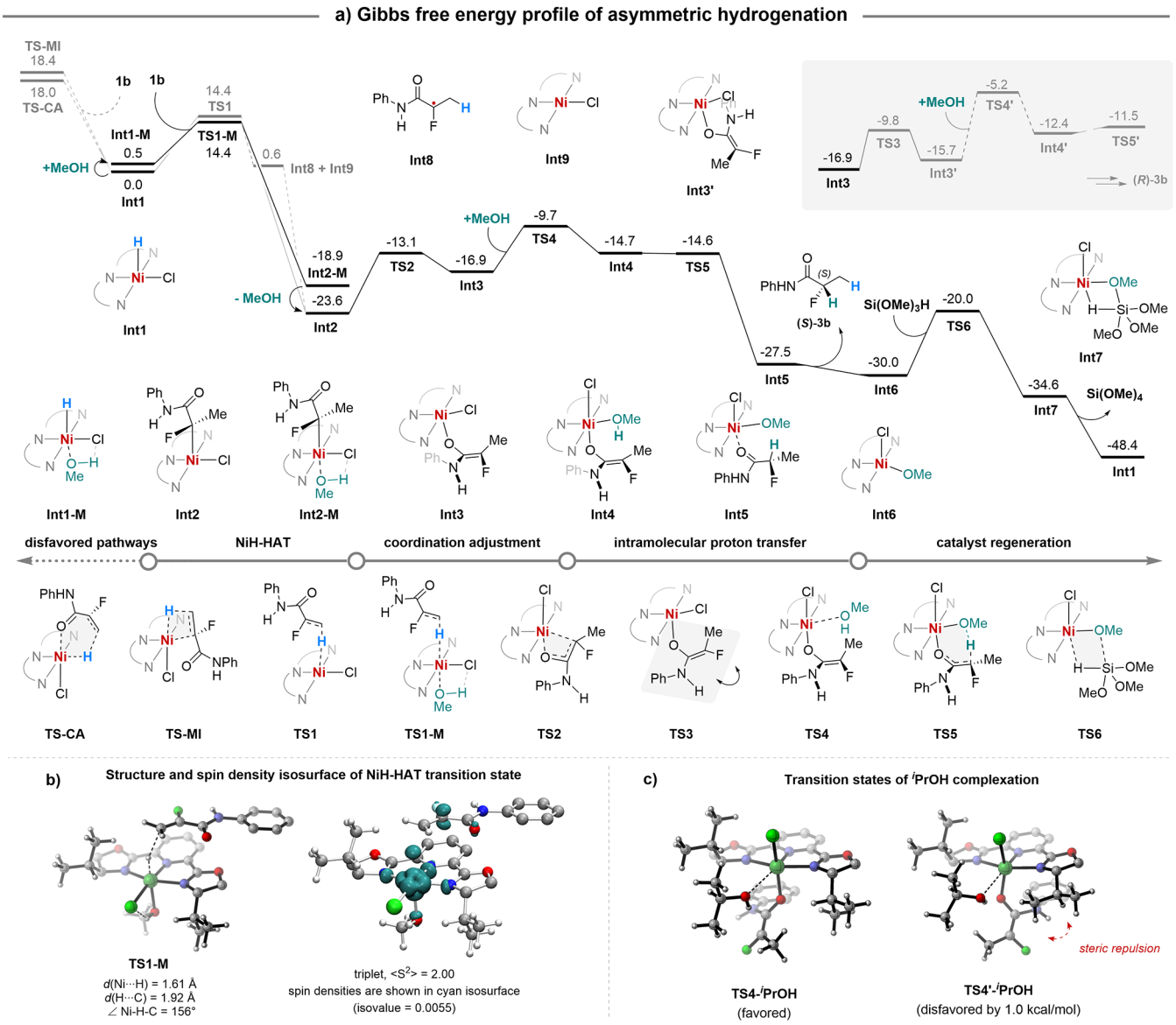

Figure 6. (a) Gibbs free energy profile of asymmetric hydrogenation (relative free energies are given in kcal/mol; **L4** and MeOH are used in computations for simplification); (b) structure and spin density isosurface of **TS1-M**; (c) relative free energies of ^{i}PrOH complexation transition states **TS4-^{i}PrOH** and **TS4′-^{i}PrOH**. Color scheme: H, white; C, gray; N, blue; O, red; F, green (small); Cl, green (medium); Ni, green (large). Some hydrogen atoms have been omitted in 3D structures for clarity.

pharmaceuticals were evaluated. As shown in Figure 4a, tertiary alkyl bromides derived from coumarin (**2as**), oxaprozin (**2at**), amino acid (**2au**), diflunisal (**2av**), chloroxylenol (**2aw**), ketoprofen (**2ax**), febuxostat (**2ay**), and probenecid (**2az**) underwent efficient couplings with alkenyl fluoride **1r** to furnish the corresponding enantioenriched secondary α-fluoro amides with moderate yields and high enantiomeric excess (up to 95% ee). Under optimal conditions for the HAT/alkyl coupling reaction (Figure 3b), primary alkyl bromides derived from isoxepac (**4o**), estrone (**4p**), and diacetonefructose (**4q**) were effective coupling partners, forging F-bearing tertiary amides with moderate yields and excellent regioselectivity (r.r. > 20:1). These experimental results demonstrate the substrate compatibility of the two radical transfer protocols. Furthermore, the resultant α-fluoro amides are useful synthetic intermediates (Figure 4b).[20] The reduction of α-fluoro amide **2n** with borane dimethylsulfide produced the chiral α-fluoro amine **5** with an ee of 91% and an overall yield of 88%.[21] α-Fluoro amide **2w** was readily converted to the corresponding chiral α-fluoro acid **6** (85% yield),[22] which condensed with phenol in the presence of dicyclohexylcarbodiimide to produce chiral α-fluoro ester **7** (90% ee, 55% overall yield for 3-steps)[23] or was reduced by $LiAlH_4$ to deliver chiral β-fluoro alcohol **8** (90% ee, 76% overall yield for 3-steps).[24]

We performed preliminary mechanistic studies to elucidate the potential reaction pathways for these asymmetric HAT and alkyl transfer reactions (Figure 5). First, deuterium-labeling experiments were performed. The hydrogenation reaction of **1n** with Ph_2SiD_2, D_2O, or CH_3OD indicated that β-hydrogen of product **3o** came from silane (98% D) while α-hydrogen of **3o** came from alcohol or water (20%−48% D) (Figure 5a). Under the standard alkyl transfer conditions, the reaction of **1n** and ^{t}BuBr with Ph_2SiD_2 produced the nondeuterated product **2n** in 81% yield and 90% ee; the parallel reaction of **1n** and

https://doi.org/10.1021/jacs.4c01506
J. Am. Chem. Soc. 2024, 146, 11418−11431

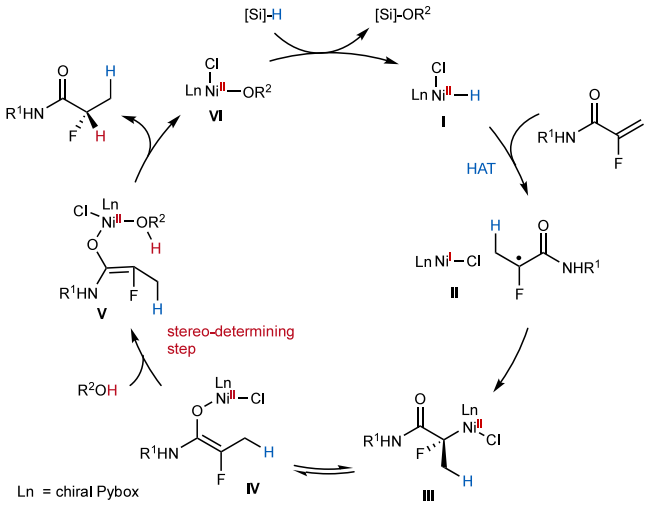

Figure 7. Proposed catalytic cycle for the NiH-HAT reaction.

^{t}BuBr with Ph_2SiH_2 and D_2O produced the α-deuterated product **D-2n** in 68% yield (40% D), together with 50% yield of α -deuterated hydrogenation product **D-3o** (42% D); similar results were obtained with the addition of MeOD (Figure 5b). These results suggested that the α-hydrogen of α-F amide products came from a proton, while silane functioned as a terminal reductant in the alkyl transfer reaction. Indeed, employing zinc or manganese powder to replace silane led to the formation of the same alkylation product **2a** in the reaction of **1a** and ^{t}BuBr, albeit with decreased yields and ee values (see Table S3 in the SI).

Similar to Norton's findings,[10c] the reduction reaction with α-CF_3 alkenyl amide **9** produced *gem*-difluoroalkene **10** with a 51% yield, confirming the H· transfer from nickel hydride; also, the reaction of **9** with ^{t}BuBr produced the alkylation/defluorination product **11** with a yield of 61% (Figure 5c).[25] Furthermore, the reaction of alkenyl fluoride **1n** with alkene-incorporated secondary alkyl iodide **12** resulted in a 33% yield of the 7-membered cyclization product **13**, which was likely generated by a radical addition followed by an intramolecular 7-*endo-trig* radical cyclization,[26] suggesting the involvement of secondary alkyl radicals (Figure 5d).

Performing the hydrogenation reaction of **1a** with Ph_2SiD_2 showed a small primary kinetic isotope effect (KIE) (1.40) on the initial rates of the reactions, which is similar to the KIE effect of FeH-HAT reported by Baran et al. (Figure 5e).[27] Comparable KIEs were observed when performing the parallel and competitive reactions with Ph_2SiD_2 (1.19 and 1.27, respectively, see Tables S27 and S28 in the SI). While an inverse KIE value of 0.83 was observed when performing the

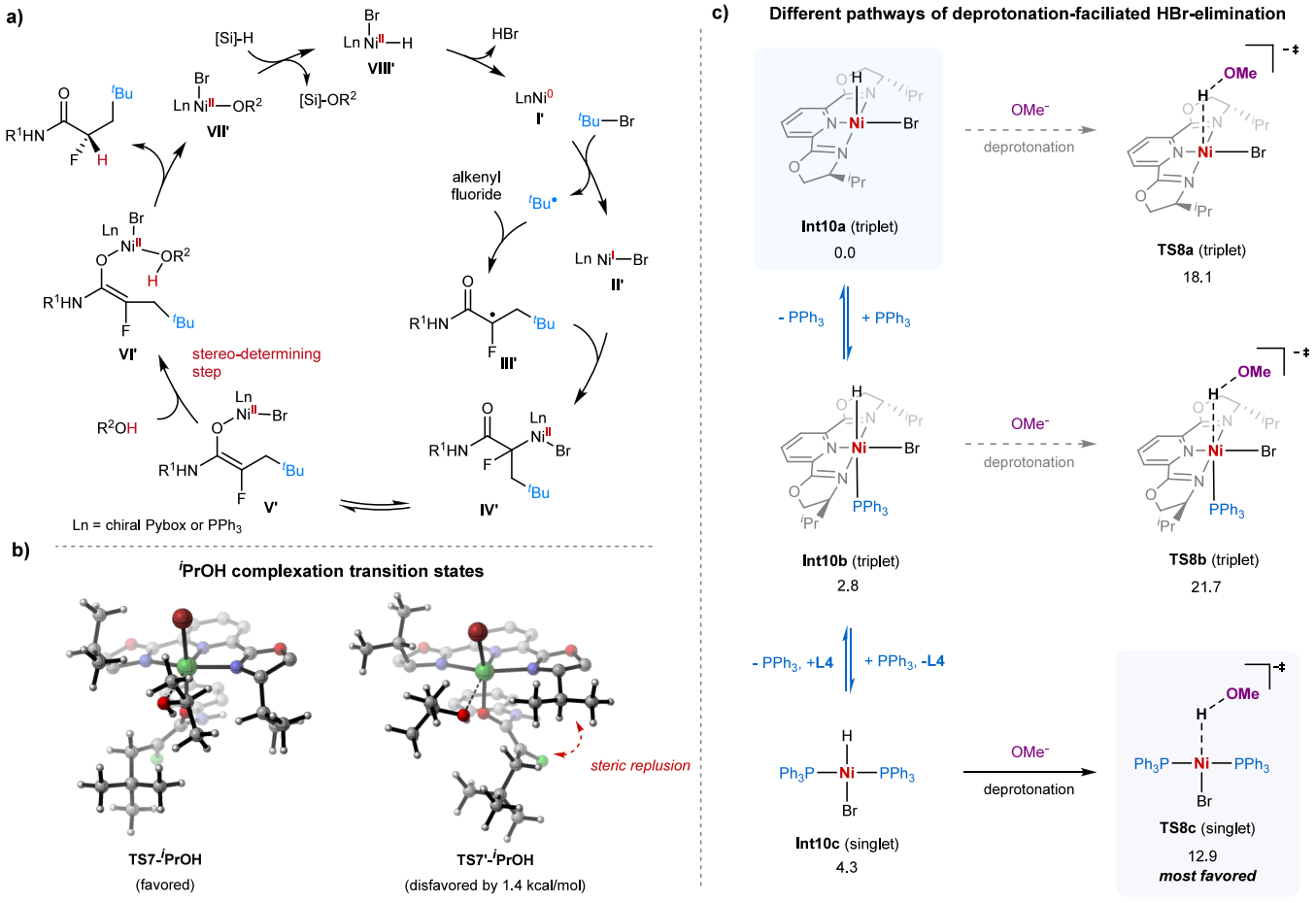

Figure 8. (a) Proposed catalytic cycle for the alkyl transfer reaction; (b) comparison of structures and relative activation free energies of ^{i}PrOH complexation transition states **TS7-^{i}PrOH** and **TS7′-^{i}PrOH**; (c) different pathways of deprotonation-facilitated HBr elimination. MeO^- is assumed to be the base in the computational model. Relative free energies are given by reference to **Int10a** in kcal/mol. Color scheme: H, white; C, gray; N, blue; O, red; F, green (small); Br, dark red; Ni, green (large). Some hydrogen atoms are omitted in 3D structures for clarity.

https://doi.org/10.1021/jacs.4c01506
J. Am. Chem. Soc. 2024, 146, 11418−11431

reaction with MeOD (Figure 5e) (see below for discussion). These results further support the involvement of a silane-enabled NiH-HAT process in the hydrogenation reaction. Kinetic studies were further performed to investigate the order of each component in the hydrogenation reaction. This reaction exhibited a first-order dependence on the concentrations of nickel, alkenyl fluoride, and alcohol, but a zero-order dependence on the concentration of silane (see Figures S5−S16; we also observed a positive-order rate dependence of K_3PO_4, probably due to the mass-transfer effect, please see the SI for details), implying that the NiH-HAT process could be rate-determining (vide infra).

Furthermore, the hydrogenation reaction of internal alkene (*Z*)-**14** with Ph_2SiD_2 was conducted to probe the stereo-determining step. The β-deuterated coupling product **15** was isolated in 43% yield with a low diastereomeric ratio of 2.6:1 (70% ee, 42% D) (Figure 5f), suggesting that proton transfer controls the stereoselectivity of α-carbon and NiH-HAT induced the chirality of β-carbon in the product.[14b,16b,18b] A similar phenomenon was observed for the alkylation reaction of internal alkenyl fluoride (*Z*)-**16** with tertiary alkyl bromide **17** under standard conditions (entry 1, Table 1) to afford β-alkylation product **18** in 37% yield with low diastereomeric selectivity (d.r. = 4.8:1) (Figure 5g), implying a same enantio-determining process. The activation free energy of the present reaction measured is 18.2 kcal·mol^{-1} (Figure S17), which is comparable to the DFT-calculated activation free energy of 14.4 kcal·mol^{-1} (see Figure 6 and discussion below).[28]

Computational Investigations. Then, we turned to DFT calculations to further probe the feasibility of both NiH-HAT and group transfer of alkyl radicals and the origin of enantioselectivity.

Asymmetric Hydrogenation Reaction. We proposed that the hydrogenation reaction starts with the generation of Ni(II)−H species **Int1**, likely with the aid of silane, isopropanol, and K_3PO_4. A direct HAT process, from **Int1** to alkenyl fluoride via **TS1**, can generate alkylnickel complex **Int2** with an activation energy of 14.4 kcal/mol. However, the observed first-order kinetics of alcohol suggested that alcohol is involved in this process. Therefore, the HAT comes from **Int1-M** to alkenyl fluoride via **TS1-M**, affording alkylnickel complex **Int2-M** with an activation energy of 13.9 kcal/mol. Thus, we propose that the reaction goes through **Int1**, **Int1-M**, **TS1-M**, **Int2-M**, and **Int2** consequently. The overall activation free energy for this rate-determining process is 14.4 kcal/mol, lower than the experimentally measured free energy by 3.8 kcal/mol. This discrepancy is probably attributed to the more complicated hydrogen binding environment of the MeOH molecule under real circumstances. Also, the entropy contribution from solvent and alcohol to this HAT could be another reason for this underestimation.

Structurally, both HAT transition states **TS1** and **TS1-M** share a quasi-linear Ni−H−C angle, similar to those of Fe−H, Co−H, and Ni−H HAT previously reported.[29] Electronic structure analysis of **TS1-M** reveals that one of the two unpaired electrons of **Int1** is distributed into alkenyl fluoride when generating α-carbonyl radical **Int8** (Figure 6b). The KIE values of Ni−H that transfer to the alkene and the proton of methanol are predicted to be 1.53 and 0.90 for **TS1-M** (see SI section 10.2.3), in agreement with experimental ones (Figure 5e). The primary KIE value in the former indicates Ni−H bond cleavage and C−H bond formation in the hydrogen atom transfer to the alkene step. The latter with an inverse KIE could be attributed to the coordination of methanol to the Ni center in **TS1-M**, leading to different vibrational frequencies of the O−H bonds. Competitive Ni−H 1,4-conjugate addition (via **TS-CA**) and migrative insertion (via **TS-MI**) show higher activation energies and can be ruled out, which agrees with the experiments.

Here, we want to point out that the NiH-HAT process takes place asymmetrically due to the use of a chiral Pybox ligand. **TS1-M** is favored over **SI-TS1** by 2.4 kcal/mol, generating C-chirality as shown in **Int2** with excellent selectivity (Figure S53). However, the stereochemistry generated in this step is lost in the following isomerization of **Int3** and **Int3′**, which is discussed below. Thus, the asymmetric NiH-HAT is not the stereodetermining step.

After NiH-HAT, a coordination change (endergonic by 6.7 kcal/mol) from alkylnickel complex **Int2** to nickel-enolate complex **Int3** is required to undergo the following protonation. A homolysis-recombination pathway was proposed, but the homolysis of **Int2**, forming free α-carbonyl radical **Int8** and Ni(I)-Cl complex **Int9**, is an uphill process of more than 23.0 kcal/mol. This is disfavored compared with the direct isomerization of **Int2** to **Int3** with an activation free energy of 10.5 kcal/mol. **Int3** can further isomerize to **Int3′** and the chirality in **Int2** generated in the HAT process is lost in this process.

MeOH coordination of **Int3** forms **Int4** via **TS4**, with a computed activation free energy of 7.2 kcal/mol. Then, a barrierless intramolecular proton transfer took place to afford **Int5**. Correspondingly, we computed **TS4'** giving the enantiomeric hydrogenation product, finding that this transition state is disfavored by 4.5 kcal/mol with respect to **TS4** (Figure 6a, upper right). Since alcohol coordination is the stereodetermining step for the present reaction, we then employed a larger basis set and used ^{i}PrOH instead of MeOH to understand the experimentally observed selectivity. To our delight, the free energy difference for the two transition states ($\Delta\Delta G^{\ddagger}$ between **TS4-^{i}PrOH** and **TS4′-^{i}PrOH**) was 1.0 kcal/mol, suggesting that the reaction has an enantiomeric excess of 73% at 0 °C (69% at 298 K), close to the experimentally measured ee of 90% (Figure 6c). The stereoselectivity can be explained in this way: in the disfavored alcohol coordination transition state **TS4′-^{i}PrOH**, the coming alcohol pushes the enol moiety (coordinated to Ni) toward the *i*-Pr side chain of Pybox ligand and experiences steric repulsion; but such a steric repulsion is absent in **TS4-^{i}PrOH**.

We must point out that **Int3** is possible to be protonated by an outer-sphere alcohol molecule directly (without forming alcohol-Ni complex), but this is strongly disfavored because an activation free energy of 19.1 kcal/mol is required (see the SI). Therefore, we ruled out this possibility.

Finally, **Int5** delivers the desired hydrogenation product (*S*)-**3b** and then undergoes a formal σ-bond metathesis (from **Int6** to **TS6** with an activation free energy of 10.0 kcal/mol) to regenerate **Int1**.[29f]

Based on these mechanistic and DFT calculation results, a catalytic cycle for the asymmetric hydrogenation reaction is depicted in Figure 7. For the HAT/alkyl coupling reaction, which presumably involves the same NiH-HAT process, corresponding DFT calculations are attached in the Supporting Information (see Figure S63).

Asymmetric Alkyl Transfer Reaction. Based on our mechanistic studies depicted in Figure 5, we reason that this reaction could proceed via a radical pathway with the alcohol

https://doi.org/10.1021/jacs.4c01506
J. Am. Chem. Soc. 2024, 146, 11418−11431

complexation as the stereodetermining step, similar to the NiH-HAT pathway. Meanwhile, KIE studies (inverse KIEs, 0.87 for Ph_2SiD_2; 0.85 for MeOD; see Figures S19 and S20 in the SI), kinetic studies (Figures S22 and S33 in the SI), and DFT calculations show that the specific reaction pathway for the asymmetric alkyl transfer reaction is more complicated. Although the Ni(I/II/III) catalytic cycle and Ni(0/I/II) catalytic cycle are postulated for the reaction, we found that, based on DFT calculations, the former one is less likely because it requires a much higher activation free energy for a six-coordinated Ni(III) complex to undergo the intramolecular proton transfer ($\Delta G^{\ddagger}$ > 40 kcal/mol, Figure S58 in the SI). The Ni(0/I/II) cycle is, therefore, depicted in Figure 8a. First, Ni(0) undergoes a Br atom abstraction with ^{t}Bu-Br to form Ni(I) species **II'** and ^{t}Bu· radical. Subsequent Giese-type addition of a ^{t}Bu·radical to alkenyl fluoride gives alkyl radical **III'**, which then recombines with **II'** to form intermediate **IV'**. Similarly to the HAT-mediated hydrogenation reaction, an isomerization of **IV'** forms intermediate **V'** followed by a stereodetermining alcohol coordination. We computed the transition states (using ^{i}PrOH), **TS7-^{i}PrOH** and **TS7′-^{i}PrOH** shown in Figure 8b, finding that $\Delta\Delta G^{\ddagger}$ = 1.4 kcal/mol, very close to the experimentally observed enantioselectivity. The enantioselectivity is the same as that shown in Figure 6c.

After alcohol coordination, an intramolecular and nearly barrierless proton transfer generates the desired chiral product and Ni(II) complex **VII'**. Then, a formal σ-bond metathesis forms Ni−H species **VIII'** (also denoted as **Int10a** in Figure 8c), which finally undergoes an HBr-elimination to regenerate Ni(0) species. We found that the presence of the PPh_3 ligand is beneficial to suppressing the competitive NiH-HAT reaction (Tables S8 and S15, and Figures S34−36) and facilitating the regeneration of Ni(0) (Figure 8c). Calculations suggest that a ligand exchange of **Int10a** by PPh_3 forms $NiH(PPh_3)_2Br$ (**Int10c**, ΔG = 4.3 kcal/mol), which then undergoes deprotonation-facilitated elimination of HBr to generate Ni(0) species (downhill by 40.3 kcal/mol) (see Figure S37 for the experimental monitoring of the ligand exchange process). This step is the most energetically favorable compared to the ones proceeding from **Int10a** or **Int10b** with ligated Pybox (Figure 8c). Then, a reverting phosphine-to-Pybox ligand exchange occurs during the recombination of **II'** and alkyl radical **III'** (see Figure S60).

CONCLUSIONS

In conclusion, we report the development of a nickel-catalyzed asymmetric radical transfer strategy for the selective functionalization of alkenyl fluorides to stereodefined alkyl fluorides. Using simple chiral nickel complexes, the asymmetric HAT, asymmetric alkyl transfer, and regioselective HAT/alkyl couplings of α-fluoro acrylamides with primary, secondary, and tertiary alkyl halides have been achieved with high efficiency and stereoselectivity, allowing for the facile and modular construction of diverse, structurally complex secondary/tertiary F-containing stereocenters. These transformations exhibit a broad substrate scope and high regio- and stereoselectivity, making them applicable to late-stage modifications. A series of mechanistic studies, including radical probe reactions, deuterium experiments, kinetic isotope effect (KIE) studies, and kinetic experiments, as well as DFT calculations, shed light on the Ni(II)-H HAT or alkyl group transfer pathways. This radical transfer method thus provides a distinct and modular approach for the exquisite assembly of structurally diverse, high-value fluorine-containing motifs, which medicinal chemists would likely embrace. The detailed mechanistic insights such as the processes of HAT from Ni(II)-H to alkenyl fluorides (rate-determining step), alcohol coordination to Ni (stereo-determining step), and nearly barrierless protonation of *in situ* formed Ni(II)-enolates are helpful for both understanding these reactions (and related ones) and designing new reactions in the future.

ASSOCIATED CONTENT

Supporting Information

The Supporting Information is available free of charge at https://pubs.acs.org/doi/10.1021/jacs.4c01506.

Experimental procedures, compound characterization, high-performance liquid chromatography spectra, and DFT calculations (PDF)

Nuclear magnetic resonance spectra (PDF)

Accession Codes

CCDC 2210184 contains the supplementary crystallographic data for this paper. These data can be obtained free of charge via www.ccdc.cam.ac.uk/data_request/cif, or by emailing data_request@ccdc.cam.ac.uk, or by contacting The Cambridge Crystallographic Data Centre, 12 Union Road, Cambridge CB2 1EZ, UK; fax: +44 1223 336033.

AUTHOR INFORMATION

Corresponding Authors

Zhi-Xiang Yu − *Beijing National Laboratory for Molecular Sciences (BNLMS), Key Laboratory of Bioorganic Chemistry and Molecular Engineering of Ministry of Education, College of Chemistry, Peking University, Beijing 100871, China;* orcid.org/0000-0003-0939-9727; Email: yuzx@pku.edu.cn

Lingling Chu − *State Key Laboratory for Modification of Chemical Fibers and Polymer Materials, College of Chemistry and Chemical Engineering, Center for Advanced Low-Dimension Materials, Donghua University, Shanghai 201620, China;* orcid.org/0000-0001-7969-0531; Email: lingling.chu1@dhu.edu.cn

Authors

Fan Chen − *State Key Laboratory for Modification of Chemical Fibers and Polymer Materials, College of Chemistry and Chemical Engineering, Center for Advanced Low-Dimension Materials, Donghua University, Shanghai 201620, China*

Qianwei Zhang − *Beijing National Laboratory for Molecular Sciences (BNLMS), Key Laboratory of Bioorganic Chemistry and Molecular Engineering of Ministry of Education, College of Chemistry, Peking University, Beijing 100871, China*

Yingying Li − *State Key Laboratory for Modification of Chemical Fibers and Polymer Materials, College of Chemistry and Chemical Engineering, Center for Advanced Low-Dimension Materials, Donghua University, Shanghai 201620, China*

Complete contact information is available at: https://pubs.acs.org/10.1021/jacs.4c01506

Author Contributions

[§]F.C. and Q.Z. contributed equally to this work. The manuscript was written through the contributions of all

authors. All authors have given approval to the final version of the manuscript.

Funding

The authors are grateful for the financial support provided by the National Natural Science Foundation of China (21971036; 21933003; 21991123) and the National Science Fund for Excellent Young Scholars (22122101).

Notes

The authors declare no competing financial interest.

■ ACKNOWLEDGMENTS

The authors are grateful for the financial support provided by the National Natural Science Foundation of China (21971036; 21933003; 21991123), the National Science Fund for Excellent Young Scholars (22122101), and the High-Performance Computing Platform of Peking University.

■ REFERENCES

(1) (a) Müller, K.; Faeh, C.; Diederich, F. Fluorine in Pharmaceuticals: Looking Beyond Intuition. *Science* **2007**, *317* (5846), 1881−1886. (b) O'Hagan, D. Understanding organofluorine chemistry. An introduction to the C-F bond. *Chem. Soc. Rev.* **2008**, *37* (2), 308−19. (c) Purser, S.; Moore, P. R.; Swallow, S.; Gouverneur, V. Fluorine in medicinal chemistry. *Chem. Soc. Rev.* **2008**, *37* (2), 320−330.

(2) (a) Mei, H.; Han, J.; Fustero, S.; Medio-Simon, M.; Sedgwick, D. M.; Santi, C.; Ruzziconi, R.; Soloshonok, V. A. Fluorine-Containing Drugs Approved by the FDA in 2018. *Chem. - Eur. J.* **2019**, *25* (51), 11797−11819. (b) Inoue, M.; Sumii, Y.; Shibata, N. Contribution of Organofluorine Compounds to Pharmaceuticals. *ACS Omega* **2020**, *5* (19), 10633−10640. (c) Silvestri, I. P.; Colbon, P. J. J. The Growing Importance of Chirality in 3D Chemical Space Exploration and Modern Drug Discovery Approaches for Hit-ID. *ACS. Med. Chem. Lett.* **2021**, *12* (8), 1220−1229.

(3) (a) Brugarolas, P.; Bhuiyan, M.; Kucharski, A.; Freifelder, R. Automated Radiochemical Synthesis of [18F]3F4AP: A Novel PET Tracer for Imaging Demyelinating Diseases. *JoVE* **2017**, No. 123, No. e55537. (b) Zhang, J.-L.; Li, Y.-H.; Wang, L.-L.; Liu, H.-Q.; Lu, S.-Y.; Liu, Y.; Li, K.; Liu, B.; Li, S.-Y.; Shao, F.-M.; Wang, K.; Sheng, N.; Li, R.; Cui, J.-J.; Sun, P.-C.; Ma, C.-X.; Zhu, B.; Wang, Z.; Wan, Y.-H.; Yu, S.-S.; Che, Y.; Wang, C.-Y.; Wang, C.; Zhang, Q.; Zhao, L.-M.; Peng, X.-Z.; Cheng, Z.; Chang, J.-B.; Jiang, J.-D. Azvudine is a thymus-homing anti-SARS-CoV-2 drug effective in treating COVID-19 patients. *Signal. Transduction. Targeted. Ther.* **2021**, *6* (1), 414.

(4) (a) Kirk, K. L. Fluorination in Medicinal Chemistry: Methods, Strategies, and Recent Developments. *Org. Process Res. Dev.* **2008**, *12* (2), 305−321. (b) Szpera, R.; Moseley, D. F. J.; Smith, L. B.; Sterling, A. J.; Gouverneur, V. The Fluorination of C−H Bonds: Developments and Perspectives. *Angew. Chem., Int. Ed.* **2019**, *58* (42), 14824−14848. (c) Britton, R.; Gouverneur, V.; Lin, J.-H.; Meanwell, M.; Ni, C.; Pupo, G.; Xiao, J.-C.; Hu, J. Contemporary synthetic strategies in organofluorine chemistry. *Nat. Rev. Methods Primers* **2021**, *1* (1), 47. (d) Leibler, I. N.-M.; Gandhi, S. S.; Tekle-Smith, M. A.; Doyle, A. G. Strategies for Nucleophilic C(sp3)−(Radio)Fluorination. *J. Am. Chem. Soc.* **2023**, *145*, 9928.

(5) (a) Ma, J.-A.; Cahard, D. Asymmetric Fluorination, Trifluoromethylation, and Perfluoroalkylation Reactions. *Chem. Rev.* **2004**, *104* (12), 6119−6146. (b) Wolstenhulme, J. R.; Gouverneur, V. Asymmetric Fluorocyclizations of Alkenes. *Acc. Chem. Res.* **2014**, *47* (12), 3560−3570. (c) Champagne, P. A.; Desroches, J.; Hamel, J.-D.; Vandamme, M.; Paquin, J.-F. Monofluorination of Organic Compounds: 10 Years of Innovation. *Chem. Rev.* **2015**, *115* (17), 9073−9174. (d) Yang, X.; Wu, T.; Phipps, R. J.; Toste, F. D. Advances in Catalytic Enantioselective Fluorination, Mono-, Di-, and Trifluoromethylation, and Trifluoromethylthiolation Reactions. *Chem. Rev.* **2015**, *115* (2), 826−870.

(6) (a) Zhu, Y.; Han, J.; Wang, J.; Shibata, N.; Sodeoka, M.; Soloshonok, V. A.; Coelho, J. A. S.; Toste, F. D. Modern Approaches for Asymmetric Construction of Carbon−Fluorine Quaternary Stereogenic Centers: Synthetic Challenges and Pharmaceutical Needs. *Chem. Rev.* **2018**, *118* (7), 3887−3964. (b) Pons, A.; Delion, L.; Poisson, T.; Charette, A. B.; Jubault, P. Asymmetric Synthesis of Fluoro, Fluoromethyl, Difluoromethyl, and Trifluoromethylcyclopropanes. *Acc. Chem. Res.* **2021**, *54* (14), 2969−2990. (c) Butcher, T. W.; Amberg, W. M.; Hartwig, J. F. Transition-Metal-Catalyzed Monofluoroalkylation: Strategies for the Synthesis of Alkyl Fluorides by C−C Bond Formation. *Angew. Chem., Int. Ed.* **2022**, *61* (7), No. e202112251.

(7) (a) Paioti, P. H. S.; Gonsales, S. A.; Xu, S.; Nikbakht, A.; Fager, D. C.; Liu, Q.; Hoveyda, A. H. Catalytic and Stereoselective Transformations with Easily Accessible and Purchasable Allyl and Alkenyl Fluorides. *Angew. Chem., Int. Ed.* **2022**, *61* (46), No. e202208742. (b) Sedgwick, D. M.; Hammond, G. B. The history and future challenges associated with the hydrogenation of vinyl fluorides. *J. Fluorine Chem.* **2018**, *207*, 45−58. (c) Ponra, S.; Yang, J.; Kerdphon, S.; Andersson, P. G. Asymmetric Synthesis of Alkyl Fluorides: Hydrogenation of Fluorinated Olefins. *Angew. Chem., Int. Ed.* **2019**, *58* (27), 9282−9287. (d) Engman, M.; Diesen, J. S.; Paptchikhine, A.; Andersson, P. G. Iridium-Catalyzed Asymmetric Hydrogenation of Fluorinated Olefins Using N,P-Ligands: A Struggle with Hydrogenolysis and Selectivity. *J. Am. Chem. Soc.* **2007**, *129* (15), 4536−4537. (e) Qu, B.; Saha, A.; Li, G.; Zeng, X.; Wang, X.; Haddad, N.; Hou, X.; Lorenz, J. C.; Wu, L.; Pennino, S.; Lee, H.; Song, J. J.; Senanayake, C. H. Large Scale Practical Synthesis of Enantiomerically Pure cis-4-Amino-3-fluoro-1-methylpiperidine via Rhodium-Catalyzed Asymmetric Hydrogenation of a Tetrasubstituted Fluoroalkene. *Org. Process Res. Dev.* **2021**, *25* (3), 583−590.

(8) Liu, J.; Yuan, Q.; Toste, F. D.; Sigman, M. S. Enantioselective construction of remote tertiary carbon−fluorine bonds. *Nat. Chem.* **2019**, *11* (8), 710−715.

(9) Li, Y.; Nie, W.; Chang, Z.; Wang, J.-W.; Lu, X.; Fu, Y. Cobalt-catalysed enantioselective C(sp3)−C(sp3) coupling. *Nat. Catal.* **2021**, *4* (10), 901−911.

(10) (a) Thornbury, R. T.; Toste, F. D. Palladium-Catalyzed Defluorinative Coupling of 1-Aryl-2,2-Difluoroalkenes and Boronic Acids: Stereoselective Synthesis of Monofluorostilbenes. *Angew. Chem., Int. Ed.* **2016**, *55* (38), 11629−11632. (b) Chen, F.; Xu, X.; He, Y.; Huang, G.; Zhu, S. NiH-Catalyzed Migratory Defluorinative Olefin Cross-Coupling: Trifluoromethyl-Substituted Alkenes as Acceptor Olefins to Form gem-Difluoroalkenes. *Angew. Chem., Int. Ed.* **2020**, *59* (13), 5398−5402. (c) Yao, C.; Wang, S.; Norton, J.; Hammond, M. Catalyzing the Hydrodefluorination of CF3-Substituted Alkenes by PhSiH3. H● Transfer from a Nickel Hydride. *J. Am. Chem. Soc.* **2020**, *142* (10), 4793−4799.

(11) (a) Iwasaki, K.; Wan, K. K.; Oppedisano, A.; Crossley, S. W. M.; Shenvi, R. A. Simple, Chemoselective Hydrogenation with Thermodynamic Stereocontrol. *J. Am. Chem. Soc.* **2014**, *136* (4), 1300−1303. (b) King, S. M.; Ma, X.; Herzon, S. B. A Method for the Selective Hydrogenation of Alkenyl Halides to Alkyl Halides. *J. Am. Chem. Soc.* **2014**, *136* (19), 6884−6887. (c) Green, S. A.; Matos, J. L. M.; Yagi, A.; Shenvi, R. A. Branch-Selective Hydroarylation: Iodoarene−Olefin Cross-Coupling. *J. Am. Chem. Soc.* **2016**, *138* (39), 12779−12782. (d) Kattamuri, P. V.; West, J. G. Hydrogenation of Alkenes via Cooperative Hydrogen Atom Transfer. *J. Am. Chem. Soc.* **2020**, *142* (45), 19316−19326.

(12) (a) Crossley, S. W. M.; Obradors, C.; Martinez, R. M.; Shenvi, R. A. Mn-, Fe-, and Co-Catalyzed Radical Hydrofunctionalizations of Olefins. *Chem. Rev.* **2016**, *116* (15), 8912−9000. (b) Wiedner, E. S.; Chambers, M. B.; Pitman, C. L.; Bullock, R. M.; Miller, A. J. M.; Appel, A. M. Thermodynamic Hydricity of Transition Metal Hydrides. *Chem. Rev.* **2016**, *116* (15), 8655−8692. (c) Green, S. A.; Crossley, S. W. M.; Matos, J. L. M.; Vásquez-Céspedes, S.; Shevick, S. L.; Shenvi, R. A. The High Chemofidelity of Metal-Catalyzed Hydrogen Atom Transfer. *Acc. Chem. Res.* **2018**, *51* (11), 2628−2640. (d) Shevick, S. L.; Wilson, C. V.; Kotesova, S.; Kim, D.;

Holland, P. L.; Shenvi, R. A. Catalytic hydrogen atom transfer to alkenes: a roadmap for metal hydrides and radicals. *Chem. Sci.* **2020**, *11* (46), 12401−12422.

(13) (a) Green, S. A.; Vásquez-Céspedes, S.; Shenvi, R. A. Iron−Nickel Dual-Catalysis: A New Engine for Olefin Functionalization and the Formation of Quaternary Centers. *J. Am. Chem. Soc.* **2018**, *140* (36), 11317−11324. (b) Shevick, S. L.; Obradors, C.; Shenvi, R. A. Mechanistic Interrogation of Co/Ni-Dual Catalyzed Hydroarylation. *J. Am. Chem. Soc.* **2018**, *140* (38), 12056−12068. (c) Zhou, X.-L.; Yang, F.; Sun, H.-L.; Yin, Y.-N.; Ye, W.-T.; Zhu, R. Cobalt-Catalyzed Intermolecular Hydrofunctionalization of Alkenes: Evidence for a Bimetallic Pathway. *J. Am. Chem. Soc.* **2019**, *141* (18), 7250−7255. (d) Song, L.; Fu, N.; Ernst, B. G.; Lee, W. H.; Frederick, M. O.; DiStasio, R. A.; Lin, S. Dual electrocatalysis enables enantioselective hydrocyanation of conjugated alkenes. *Nat. Chem.* **2020**, *12* (8), 747−754. (e) Li, Y.; Liu, W.; Liu, Z.-Y.; Wang, C.-Y.; Bian, K.-J.; Sheng, J.; Wang, X.-S. Development of Monofluoroalkenes as Molecular Platform for Diversity-Oriented Syntheses of Tertiary Aliphatic Fluorides via Nickel/Manganese-Dual Catalysis. *CCS Chem.* **2022**, *4* (9), 2888−2896.

(14) (a) Zhu, S.; Zhao, X.; Li, H.; Chu, L. Catalytic three-component dicarbofunctionalization reactions involving radical capture by nickel. *Chem. Soc. Rev.* **2021**, *50* (19), 10836−10856. (b) Guo, L.; Yuan, M.; Zhang, Y.; Wang, F.; Zhu, S.; Gutierrez, O.; Chu, L. General Method for Enantioselective Three-Component Carboarylation of Alkenes Enabled by Visible-Light Dual Photoredox/Nickel Catalysis. *J. Am. Chem. Soc.* **2020**, *142* (48), 20390−20399. (c) Tu, H.-Y.; Wang, F.; Huo, L.; Li, Y.; Zhu, S.; Zhao, X.; Li, H.; Qing, F.-L.; Chu, L. Enantioselective Three-Component Fluoroalkylarylation of Unactivated Olefins through Nickel-Catalyzed Cross-Electrophile Coupling. *J. Am. Chem. Soc.* **2020**, *142* (21), 9604−9611. (d) Li, X.; Yuan, M.; Chen, F.; Huang, Z.; Qing, F.-L.; Gutierrez, O.; Chu, L. Three-component enantioselective alkenylation of organophosphonates via nickel metallaphotoredox catalysis. *Chem.* **2023**, *9* (1), 154−169. (e) Wang, F.; Pan, S.; Zhu, S.; Chu, L. Selective Three-Component Reductive Alkylalkenylation of Unbiased Alkenes via Carbonyl-Directed Nickel Catalysis. *ACS Catal.* **2022**, *12* (15), 9779−9789.

(15) Song, P.; Zhu, S. Nickel-Catalyzed Hydrofluorination of Unactivated Alkenes through a HAT Pathway. *ACS Catal.* **2020**, *10* (22), 13165−13170.

(16) (a) Fan, C.; Zhou, Q.-L. Nickel-catalyzed group transfer of radicals enables hydrocyanation of alkenes and alkynes. *Chem. Catal.* **2021**, *1* (1), 117−128. (b) Qi, X.; Jambu, S.; Ji, Y.; Belyk, K. M.; Panigrahi, N. R.; Arora, P. S.; Strotman, N. A.; Diao, T. Late-Stage Modification of Oligopeptides by Nickel-Catalyzed Stereoselective Radical Addition to Dehydroalanine. *Angew. Chem., Int. Ed.* **2022**, *61* (48), No. e202213315.

(17) (a) Tasker, S. Z.; Standley, E. A.; Jamison, T. F. Recent advances in homogeneous nickel catalysis. *Nature* **2014**, *509* (7500), 299−309. (b) Ananikov, V. P. Nickel: The "Spirited Horse" of Transition Metal Catalysis. *ACS Catal.* **2015**, *5* (3), 1964−1971. (c) Choi, J.; Fu, G. C. Transition metal−catalyzed alkyl-alkyl bond formation: Another dimension in cross-coupling chemistry. *Science* **2017**, *356* (6334), No. eaaf7230. (d) Ogoshi, S. *Nickel Catalysis in Organic Synthesis: Methods and Reactions*; John Wiley & Sons: New York. 2020.

(18) (a) Wang, X.-X.; Lu, X.; Li, Y.; Wang, J.-W.; Fu, Y. Recent advances in nickel-catalyzed reductive hydroalkylation and hydroarylation of electronically unbiased alkenes. *Sci. China. Chem.* **2020**, *63* (11), 1586−1600. (b) Zhang, Z.; Bera, S.; Fan, C.; Hu, X. Streamlined Alkylation via Nickel-Hydride-Catalyzed Hydrocarbonation of Alkenes. *J. Am. Chem. Soc.* **2022**, *144* (16), 7015−7029. (c) Wang, Y.; He, Y.; Zhu, S. NiH-Catalyzed Functionalization of Remote and Proximal Olefins: New Reactions and Innovative Strategies. *Acc. Chem. Res.* **2022**, *55* (23), 3519−3536. (d) Yang, P.-F.; Shu, W. Asymmetric alkyl-alkyl cross-coupling enabled by earth-abundant metal-catalyzed hydroalkylations of olefins. *Chem. Catal.* **2023**, *3* (4), No. 100508.

(19) (a) Lu, X.; Xiao, B.; Zhang, Z.; Gong, T.; Su, W.; Yi, J.; Fu, Y.; Liu, L. Practical carbon−carbon bond formation from olefins through nickel-catalyzed reductive olefin hydrocarbonation. *Nat. Commun.* **2016**, *7* (1), 11129. (b) Wang, Z.; Yin, H.; Fu, G. C. Catalytic enantioconvergent coupling of secondary and tertiary electrophiles with olefins. *Nature* **2018**, *563* (7731), 379−383. (c) Zhou, F.; Zhang, Y.; Xu, X.; Zhu, S. NiH-Catalyzed Remote Asymmetric Hydroalkylation of Alkenes with Racemic α-Bromo Amides. *Angew. Chem., Int. Ed.* **2019**, *58* (6), 1754−1758. (d) Bera, S.; Mao, R.; Hu, X. Enantioselective C(sp3)−C(sp3) cross-coupling of non-activated alkyl electrophiles via nickel hydride catalysis. *Nat. Chem.* **2021**, *13* (3), 270−277. (e) Shi, L.; Xing, L.-L.; Hu, W.-B.; Shu, W. Regio- and Enantioselective Ni-Catalyzed Formal Hydroalkylation, Hydrobenzylation, and Hydropropargylation of Acrylamides to α-Tertiary Amides. *Angew. Chem., Int. Ed.* **2021**, *60* (3), 1599−1604. (f) Sun, S.-Z.; Cai, Y.-M.; Zhang, D.-L.; Wang, J.-B.; Yao, H.-Q.; Rui, X.-Y.; Martin, R.; Shang, M. Enantioselective Deaminative Alkylation of Amino Acid Derivatives with Unactivated Olefins. *J. Am. Chem. Soc.* **2022**, *144* (3), 1130−1137. (g) Wang, J.-W.; Li, Z.; Liu, D.; Zhang, J.-Y.; Lu, X.; Fu, Y. Nickel-Catalyzed Remote Asymmetric Hydroalkylation of Alkenyl Ethers to Access Ethers of Chiral Dialkyl Carbinols. *J. Am. Chem. Soc.* **2023**, *145*, 10411.

(20) (a) Yoder, N. C.; Kumar, K. Fluorinated amino acids in protein design and engineering. *Chem. Soc. Rev.* **2002**, *31* (6), 335−341. (b) Salwiczek, M.; Nyakatura, E. K.; Gerling, U. I. M.; Ye, S.; Koksch, B. Fluorinated amino acids: compatibility with native protein structures and effects on protein−protein interactions. *Chem. Soc. Rev.* **2012**, *41* (6), 2135−2171.

(21) Webb, T. H.; Wilcox, C. S. Improved synthesis of symmetrical and unsymmetrical 5,11-methanodibenzo[b,f][1,5]diazocines. Readily available nanoscale structural units. *J. Org. Chem.* **1990**, *55* (1), 363−365.

(22) (a) Evans, D. A.; Aye, Y.; Wu, J. Asymmetric, anti-Selective Scandium-Catalyzed Sakurai Additions to Glyoxyamide. Applications to the Syntheses of N-Boc d-Alloisoleucine and d-Isoleucine. *Org. Lett.* **2006**, *8* (10), 2071−2073. (b) Sharma, P.; Liu, R.-S. [3 + 2]-Annulations of N-Hydroxy Allenylamines with Nitrosoarenes: One-Pot Synthesis of Substituted Indole Products. *Org. Lett.* **2016**, *18* (3), 412−415.

(23) Toshima, H.; Maru, K.; Saito, M.; Ichihara, A. Total syntheses of cepaciamides A and B, novel fungitoxic 3-amino-2-piperidinone-containing lipids produced by Pseudomonas cepacia D-202. *Tetrahedron* **1999**, *55* (18), 5793−5808.

(24) Alvarado, J.; Herrmann, A. T.; Zakarian, A. Stereoselective α-Fluorination of N-Acyloxazolidinones at Room Temperature within 1 h. *J. Org. Chem.* **2014**, *79* (13), 6206−6220.

(25) Lu, X.; Wang, X.-X.; Gong, T.-J.; Pi, J.-J.; He, S.-J.; Fu, Y. Nickel-catalyzed allylic defluorinative alkylation of trifluoromethyl alkenes with reductive decarboxylation of redox-active esters. *Chem. Sci.* **2019**, *10* (3), 809−814.

(26) Justicia, J.; Oller-López, J. L.; Campaña, A. G.; Oltra, J. E.; Cuerva, J. M.; Buñuel, E.; Cárdenas, D. J. 7-endo Radical Cyclizations Catalyzed by Titanocene(III). Straightforward Synthesis of Terpenoids with Seven-Membered Carbocycles. *J. Am. Chem. Soc.* **2005**, *127* (42), 14911−14921.

(27) Lo, J. C.; Kim, D.; Pan, C.-M.; Edwards, J. T.; Yabe, Y.; Gui, J.; Qin, T.; Gutiérrez, S.; Giacoboni, J.; Smith, M. W.; Holland, P. L.; Baran, P. S. Fe-Catalyzed C−C Bond Construction from Olefins via Radicals. *J. Am. Chem. Soc.* **2017**, *139* (6), 2484−2503.

(28) Cho, K.; Kim, E. J.; Seo, M. S.; Shaik, S.; Nam, W. Correlating DFT-Calculated Energy Barriers to Experiments in Nonheme Octahedral FeIVO Species. *Chem. - Eur. J.* **2012**, *18* (33), 10444−10453.

(29) (a) Jiang, H.; Lai, W.; Chen, H. Generation of Carbon Radical from Iron-Hydride/Alkene: Exchange-Enhanced Reactivity Selects the Reactive Spin State. *ACS Catal.* **2019**, *9* (7), 6080−6086. (b) Kim, D.; Rahaman, S. M. W.; Mercado, B. Q.; Poli, R.; Holland, P. L. Roles of Iron Complexes in Catalytic Radical Alkene Cross-Coupling: A Computational and Mechanistic Study. *J. Am. Chem. Soc.*

https://doi.org/10.1021/jacs.4c01506
J. Am. Chem. Soc. 2024, 146, 11418−11431

2019, *141* (18), 7473−7485. (c) Wahidur Rahaman, S. M.; Matyjaszewski, K.; Poli, R. Cobalt(iii) and copper(ii) hydrides at the crossroad of catalysed chain transfer and catalysed radical termination: a DFT study. *Polym. Chem.* **2016**, *7* (5), 1079−1087. (d) de Bruin, B.; Dzik, W. I.; Li, S.; Wayland, B. B. Hydrogen-Atom Transfer in Reactions of Organic Radicals with [CoII(por)]. (por = Porphyrinato) and in Subsequent Addition of [Co(H)(por)] to Olefins. *Chem. - Eur. J.* **2009**, *15* (17), 4312−4320. (e) Kamei, Y.; Seino, Y.; Yamaguchi, Y.; Yoshino, T.; Maeda, S.; Kojima, M.; Matsunaga, S. Silane- and peroxide-free hydrogen atom transfer hydrogenation using ascorbic acid and cobalt-photoredox dual catalysis. *Nat. Commun.* **2021**, *12* (1), 966. (f) Guo, J.; Zhang, D.; Wang, X. Mechanistic insights into Ni-catalyzed hydrogen atom transfer (HAT)-triggered hydrodefluorination of CF3-substituted alkenes. *Dalton Trans.* **2021**, *50* (26), 9026−9030.

https://doi.org/10.1021/jacs.4c01506
J. Am. Chem. Soc. 2024, 146, 11418−11431